Hindawi
Geofluids
Volume 2019, Article ID 9021586, 12 pages
https://doi.org/10.1155/2019/9021586

*Research Article*

# The Relationship between Current Ground Stress and Permeability of Coal in Superimposed Zones of Multistage Tectonic Movement

**Xiaoming Ni**,[1,2] **Qifeng Jia**,[1] **and Yanbin Wang**[3]

[1]*School of Energy Science and Engineering, Henan Polytechnic University, Jiaozuo, China*
[2]*Collaborative Innovation Center of Coalbed Methane and Shale Gas for Central Plains Economic Region, Henan Province, Jiaozuo, China*
[3]*College of Geoscience and Surveying Engineering, China University of Mining & Technology, Beijing, China*

Correspondence should be addressed to Qifeng Jia; 211602020019@home.hpu.edu.cn

Received 1 November 2018; Revised 2 January 2019; Accepted 16 January 2019; Published 10 April 2019

Academic Editor: Micòl Mastrocicco



According to the characteristics of the paleostress field and tectonic features at the key moments during tectonic movement after the formation of the no. 3 coal seam, the superimposed areas of different folding zones in the southern section of Shizhuang in central and southern Qinshui Basin were divided. The reservoir permeability of the coal in different superimposed areas was obtained by integrating a laboratory in situ measurement technique, geological strength indices, and multiple parameter fitting of acoustic logging data. The maximum and minimum horizontal principal stresses in different superimposed areas were gained through analysis of the fracturing curve and acoustic logging data. Thus, the relationships between ground stress and permeability in different superimposed areas were revealed. The results show that the relationships between different stresses and permeability were not obvious without considering multistage tectonic superposition. The relationships between the varying stresses and permeability in the same superimposed areas were exponential. The deformation of coal seams in the superimposed areas on the wings of fold belts striking north-central direction was relatively weak, and its permeability was the highest. The permeability in the superimposed areas of the wings of different fold belts in a southeasterly direction was lower than that in the superimposed areas of the wings and the cores of folds. The permeability is the worst in the superimposed areas by the cores and wings of the folds. The results can provide a reference for the study of the heterogeneous deformation of coal reservoirs.

## 1. Introduction

Tectonic movement is one of the necessary conditions for the formation of coal seams, which not only affects the thickness and form of a coal seam but also affects the current stress regime. The current stress and palaeotectonic stress can jointly control the permeability of a coal seam. In recent years, existing studies have found the permeability of coal seams by using methods including laboratory or in situ measurement, acoustic well logging, and integrated *in situ* well measurements [1–3] and estimated stresses by numerical simulation based on ANSYS with calculation of hydraulic fracturing pressure curves, strain gauge measurement [4–6], etc. Based on the relationship between permeability and ground stress, the changes in permeability are exponentially related to the change in ground stress [7]. According to this relationship, a high-permeability zone was predicted [8, 9]. Their predicted results are relatively accurate when applied in relatively simple areas with regard to geological structure and coalbed deformation [10]. However, with multiple tectonic movements and the relatively complicated geological structural conditions in most of China [11–15], there may be superimposed areas of "the cores of different synclines, the wings and the cores of different synclines, the cores of different anticlines, the wings and the cores of different anticlines, different wings of the folds" involved in the deformation of coal seams due to the differences in the directions of the principal stresses during multistage tectonic movement;

this changes the stress state, and therefore, the same formula may not be suitable for illustrating the relationship between permeability and ground stress. Laboratory and in situ measurement techniques, or acoustic well logging, exhibit shortfalls including high cost and the need for a large number of samples for statistical analysis of the relationship between permeability and stress [16–18]. The removal of outliers has an important influence on the fitting result when integrating acoustic logging analysis and *in situ* measurement [19, 20]. Based on the results from the ANSYS software, the selected parameters such as stiffness ratio and cohesion have an important effect [21–23]. The curves of hydraulic fracturing measurement were used to calculate ground stress; however, the abnormal curves of hydraulic fracturing tend to affect the values of the key parameters such as fracture pressure and pressure of transient pump stopping, consequently influencing the accuracy of the calculated ground stress. When the ground stress was calculated from the logging curve, the selection of tectonic stress coefficients affects the result, which may differ greatly from real values. This research used the method of identifying coal structure by acoustic logging analysis and core drilling; the geological strength index (GSI) was evaluated in this research of coal deformation. Based on the relationship between permeability and GSI, the permeability in different superimposed zones was obtained based on the relationship between multiple-parameter logging and GSI. The relationship between different stresses and permeability in different superimposed zones was obtained during hydraulic fracturing. The results of this study provide a reference for the prediction of permeabilities in superimposed zones under multistage tectonic movement.

## 2. Geological Background to the Study Area

The southern section of Shizhuang is relatively active region of coalbed methane (CBM) development in the central and southern areas of Qinshui Basin with an area of 336 $km^2$. Coal seam dip angles are 3° in monoclinal structures inclined to the west [24]. According to its complexity, it can be divided into southern, central, and northern regions; this study is only based on the central region. The strata formed are Paleozoic Permian, Mesozoic, Triassic, Neogene Tertiary, and Quaternary [25]. Among them, the no. 3 coal seams from the Permian in the Shanxi Group form the main coal seams subjected to CBM development in this area. No. 3 coal seam, after being formed, experienced extrusion stresses in a SN direction arising from the Indosinian movement, NW-SE from the Yanshanian movement, NNE-SSW from the early Himalayan movement, and NEE-SWW from the late Himalayan movement. As tectonic movements in the Indosinian period exert insignificant effects on tectonic deformation on these coal seams, they are not discussed further. Coal seams subjected to the effect of tectonic movements in the Yanshanian period (Late Mesozoic) formed superimposed zones of alternatively overlaid anticlines and synclines. Different tectonic zones are known as the wings and cores of anticlines or synclines. Furthermore, the coal seams, under the effect of tectonic movement in the Himalayan period, also formed alternatively overlaid anticlines and synclines. Different zones with superimposed folds were formed by the deformed coal seams after being subjected to the effect of tectonic movement in the Yanshanian and Himalayan periods, respectively. Considering the tectonic movements in different periods, the research area was divided into multiple superimposed zones including "the cores of different synclines (Zone I), the wings and the core of different anticlines (Zone II), the cores of different anticlines (Zone III), the wings of different synclines or anticlines, (Zone IV, in the north-central direction), the wings of different synclines or anticlines, (Zone V, in the southeast direction), the wings and the cores of different anticlines (Zone VI)." The no. 3 coal seam in this area is generally between 3.69 m and 9.95 m thick, the gas content is generally between 8.0 $m^3$/t and 25.6 $m^3$/t, and the depth of the coal seam is between 600 m and 950 m. The superimposed partition of different tectonic regions in the central of the southern part of Shizhuang is shown in Figure 1.

## 3. Research Method

It is concluded that the numerical values of ground stress and permeability are needed in the study of the relationship between current ground stress and permeability. The method of obtaining the permeability of these coal reservoirs is as follows: firstly, the coal core samples drilled in some CBM wells in the research area were observed and compared with their logging curves and the values of logging responses of different coal structures were obtained. Then, the modified GSI was used to calibrate each coal sample and fit the logging response of multiple parameters from well test technology so as to build the relationship between them. Additionally, the relationship between GSI and the permeability of coal cores was obtained through the permeability testing of coal cores. Finally, the permeability was calculated according to the multiple parameters obtained by acoustic well logging in the superimposed zone.

The method of measuring ground stress is as follows: the abnormal curve of high pressures in the fracturing construction process was excluded and relatively standardised construction curves from hydraulic fracturing operations were selected. According to the principle of ground stress measured by hydraulic fracturing, the maximum and minimum principal stresses were calculated based on the tensile strength obtained by laboratory testing. Using acoustic logging to calculate the ground stress, combined with that determined during hydraulic fracturing, the tectonic ground stress coefficients in different superimposed regions were obtained. On this basis, the maximum and minimum principal ground stresses in an abnormal well of the fracturing construction curve were obtained and the maximum and minimum principal ground stresses in each CBM well in different superimposed areas were calculated. Finally, the differences between ground stresses and permeabilities were fitted in different superimposed zones and the corresponding relationships were obtained.

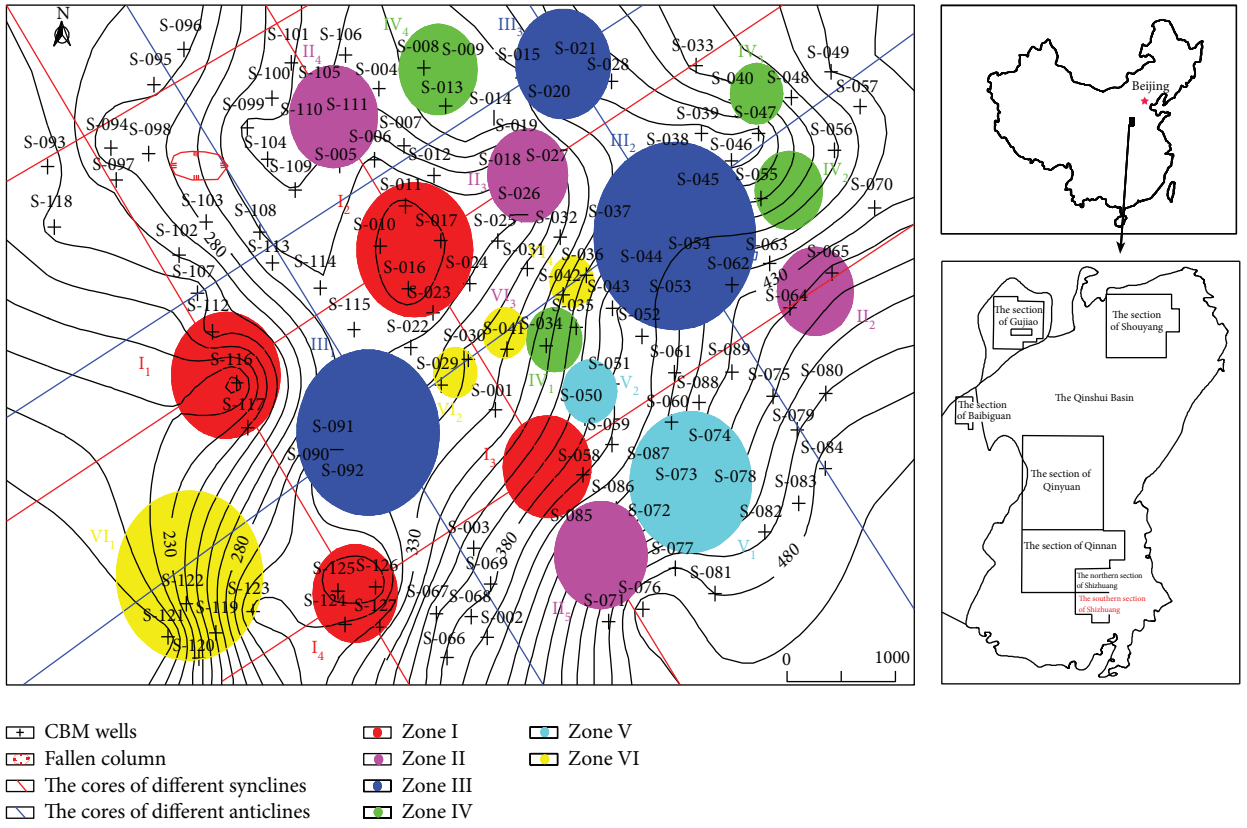


Figure 1: The superimposed partition of different tectonic regions in the central of the southern part of Shizhuang.

## 4. Results and Discussion

### 4.1. The Permeability of the Coal Reservoir and Calculation of Current Ground Stress

*4.1.1. Quantitative Characterisation of Coal Structure Based on GSI.* Coal structure is usually classified using the method based on its deformation into class I coal (primary structure coal), class II coal (fragmented coal), class III coal (granulated coal), and class IV coal (mylonitised coal) [25]. This classification method is relatively old. Hoek and Brown [26] estimated the strength of a rock mass according to its mechanical properties and the roughness of the rock surface. Coal seams can also be considered as a rock mass. Some scholars have adopted the width and filling of cracks in coal to replace the weathering of structural planes in the traditional GSI chart. Based on the gradual transition process of coal deformation, combined with GSI, the deformation degree of coal is described quantitatively and finely [27–29]. The GSI value gradually decreased from primary structure coal to mylonitised coal. The quantitative characterisation of coal structure was conducted (Figure 2) according to GSI revised by reference [27].

A correlation was made between the typical parameters in the logging curve and the GSI values (Figures 3(a)–3(d)).

There is a certain relationship between GSI and a single factor, but the correlation was not high. To improve prediction accuracy, the multiparameter formula for the GSI was established as follows:

$$\mathrm{GSI} = a\mathrm{DEN} + b\mathrm{GR} + c\mathrm{CALX} + d\mathrm{CALY} + e. \quad (1)$$

The coefficients are calculated by fitting: $a = 72.946$, $b = 1.230$, $c = -6.873$, $d = 6.538$, $e = -77.588$, $R^2 = 0.762$, and $\mathrm{sig} = 0.004 < 0.005$; the prediction accuracy was thus improved.

According to (1), the GSI values of the coal seam in different structural parts were judged. The GSI values for the coal seam section of typical CBM wells are shown in Figure 4.

The GSI values of the coal with strong heterogeneity along the longitudinal direction were found to be 1 m; then, the average value was used as the GSI value for that well. The GSI values of CBM wells in different superimposed tectonic zones can thus be obtained.

*4.1.2. Calculation of Permeability in Different Tectonic Superimposed Zones.* The permeability of coal samples at different GSI values was calculated, and the relationship between GSI value and permeability was obtained, as shown in Figure 5; when the GSI value is 55.03, the permeability is maximised, while the coal seams are intact, and when fractured, the permeability increases.

Through the calculation of the GSI value of CBM wells in different superimposed areas, the permeability can be

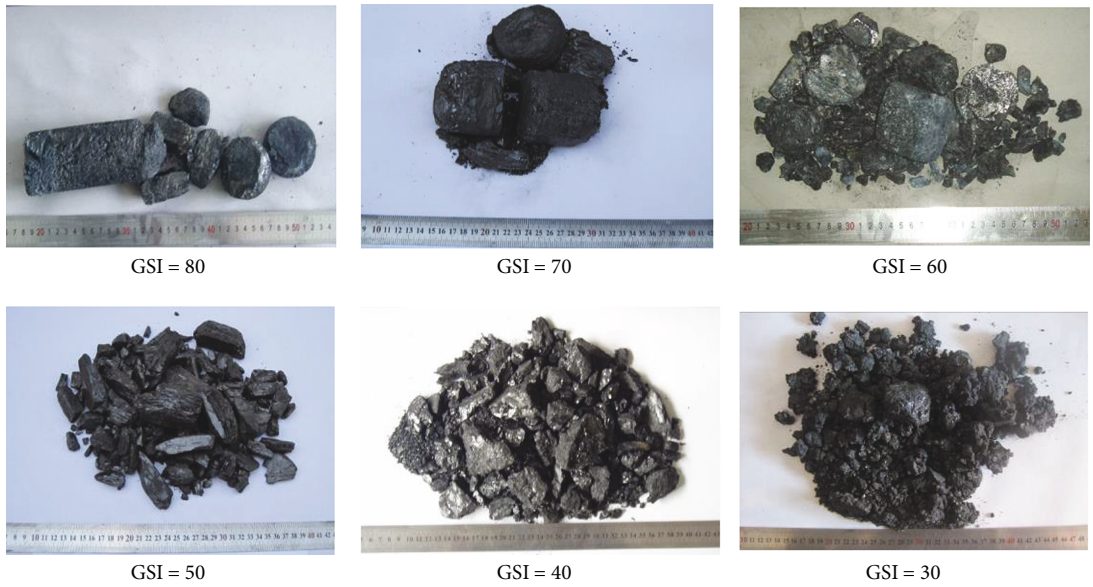


Figure 2: GSI quantisation of coal showing typical deformation in the study area.

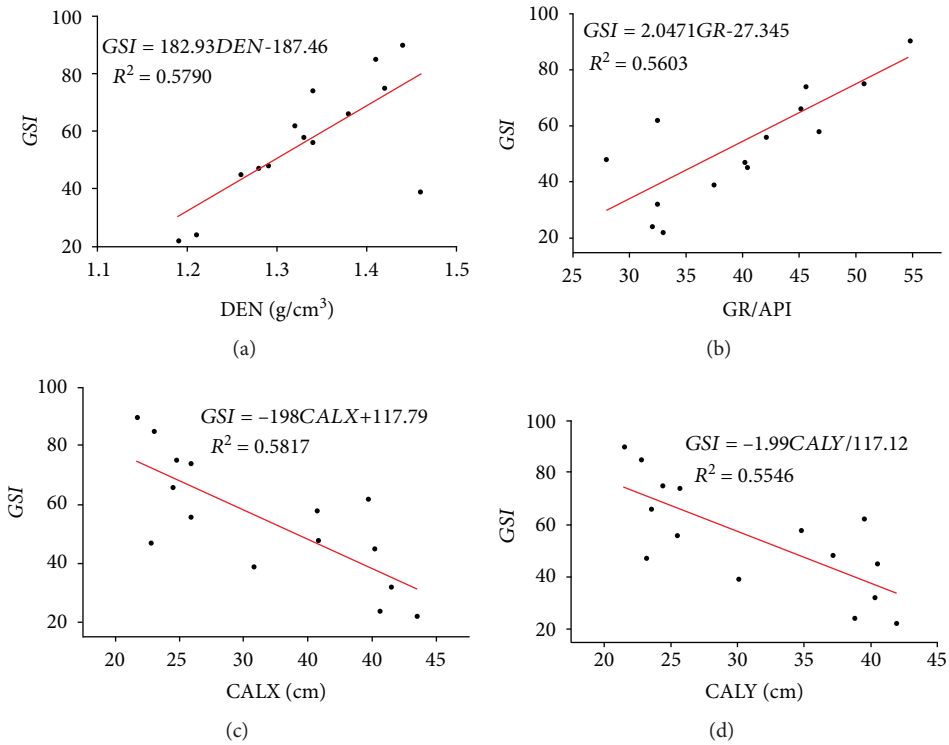


Figure 3: (a) The relationship between volume density and GSI. (b) The relationship between natural gamma ray and GSI. (c) The relationship between borehole diameter of the X direction and GSI. (d) The relationship between borehole diameter of the Y direction and GSI.

calculated based on the relationship between permeability and GSI values (Table 1); the permeability of coal seams in the superimposed areas of different tectonic regions varied. The permeability of coal seams was the lowest in the superimposed regions formed by the cores of different synclines or anticlines.

### 4.2. The Calculated Current Ground Stress in Different Superimposed Areas under Multistage Tectonic Movement

*4.2.1. Hydraulic Fracturing to Calculate Ground Stress.* As a method of measuring ground stress, hydraulic fracturing was mainly applied to calculate the maximum and minimum

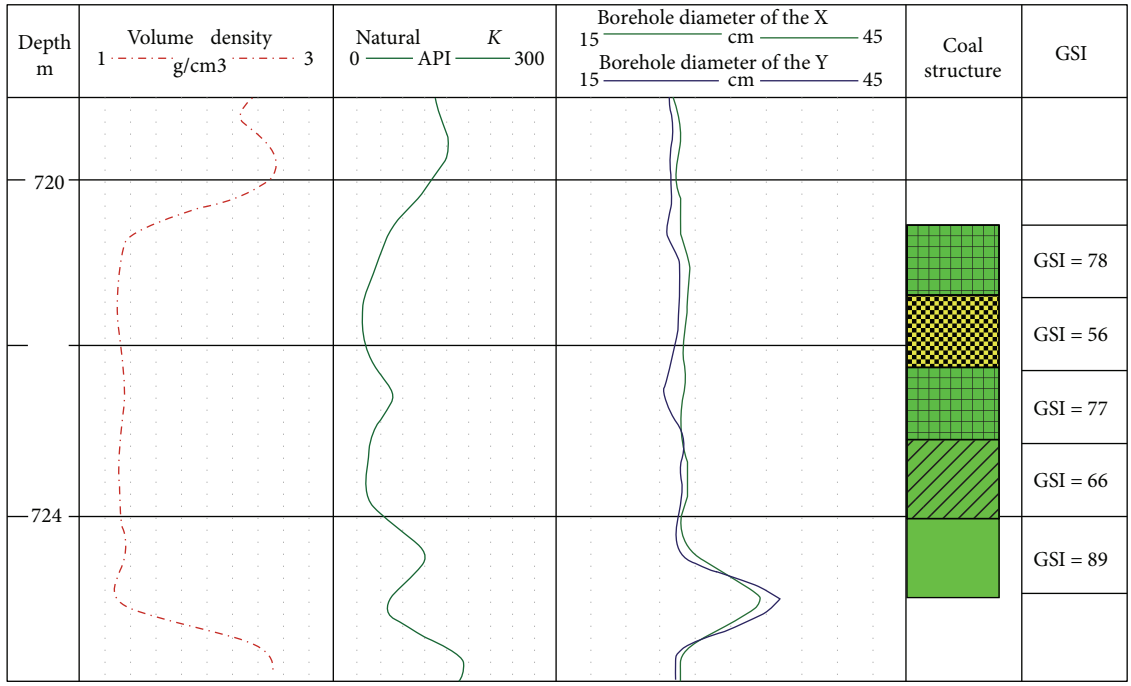


Figure 4: The GSI values for the coal seam section of typical CBM wells.

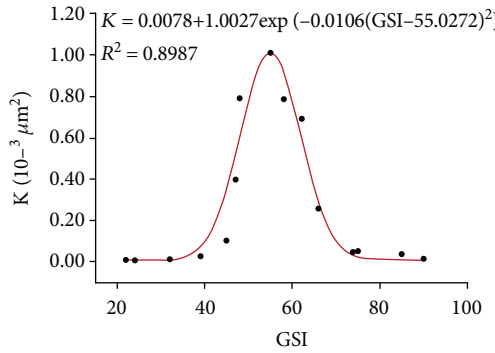


Figure 5: The relationship between GSI value and permeability.

principal stresses based on the following assumptions: fractured rock formations are linear, homogeneous, isotropic, and elastomers. The initial fracture surface under the effect of hydraulic fracturing is upright and parallel to the orifice. There is a long section of the fracture surface perpendicular to the minimum horizontal principal ground stress direction. The maximum horizontal principal stress and minimum horizontal principal stress can be expressed as follows [30, 31]:

$$\begin{cases} \sigma_H = 3\sigma_h - p_f - p_0 + s_t, \\ \sigma_h = p_{ISTP}, \end{cases} \quad (2)$$

where $\sigma_H$ is the maximum principal stress, MPa; $\sigma_h$ denotes the minimum horizontal principal stress, MPa; $p_f$ represents the pressure on the coal to be fractured, MPa; $p_0$ is the pressure on the coal reservoir, MPa; $s_t$ denotes the tensile strength of the coal, MPa; and $p_{ISTP}$ can be read directly from the hydraulic fracturing curve.

When the hydraulic fracturing construction curve is normal, the minimum and maximum principal stresses can be calculated based on the fracture pressure from the hydraulic fracturing curve, instantaneous shut-in pressure, and tensile strength of the coal. However, the fracture pressure in hydraulic fracturing was higher than the actual value when drilling causes the hole diameter of the coal seam section to expand or cementing causes some pollution to the near-wellbore zone. Furthermore, unreasonable pump injection during the fracturing process may cause the pressure to rise, which in turn causes the instantaneous shut-in pressure of pump to rise; this is inconsistent with actual cases. In this case, the maximum and minimum principal stresses are often inaccurate. The oil pressure curve in the normal fracturing operation curve has a small drop from the rupture pressure to the instantaneous shut-in pressure, and the curve is smooth. However, the oil pressure curve in the abnormal fracturing operation curve decreased greatly from the rupture pressure to the instantaneous shut-in pressure, and the curve was bent up and down and not smooth enough. The abnormal and normal fracturing construction curves are shown in Figures 6(a) and 6(b), respectively. $p_f$ and $p_{ISTP}$, respectively, represent the rupture pressure and instantaneous shut-in pressure.

According to formula (2), the fracturing pressure and instantaneous shut-in pressure of the hydraulic pump could be read to find the maximum and minimum principal stresses.

*4.2.2. Ground Stress Obtained by Acoustic Logging and Hydraulic Fracturing Techniques.* During fracturing, the fracturing pressure on abnormal CBM wells and the value of

Table 1: The average GSI value and permeability of partial CBM wells in different structural superposition zones.

| Zones | Well number | The average GSI value | Permeability ($10^{-3}$ $\mu m^2$) |
|---|---|---|---|
| $I_2$ | S-010 | 35 | 0.026 |
| $I_2$ | S-011 | 38 | 0.056 |
| $I_3$ | S-058 | 33 | 0.015 |
| $I_1$ | S-117 | 28 | 0.008 |
| $I_4$ | S-124 | 33 | 0.013 |
| $II_4$ | S-005 | 68 | 0.160 |
| $II_3$ | S-018 | 70 | 0.110 |
| $II_4$ | S-019 | 69 | 0.120 |
| $II_2$ | S-064 | 69 | 0.121 |
| $II_1$ | S-085 | 66 | 0.321 |
| $III_3$ | S-015 | 38 | 0.052 |
| $III_3$ | S-020 | 39 | 0.083 |
| $III_2$ | S-044 | 36 | 0.028 |
| $III_2$ | S-062 | 35 | 0.021 |
| $III_1$ | S-090 | 38 | 0.062 |
| $IV_4$ | S-008 | 74 | 0.030 |
| $IV_4$ | S-013 | 69 | 0.120 |
| $IV_1$ | S-034 | 64 | 0.471 |
| $IV_1$ | S-035 | 60 | 0.760 |
| $IV_3$ | S-040 | 72 | 0.052 |
| $V_2$ | S-050 | 36 | 0.033 |
| $V_2$ | S-051 | 38 | 0.060 |
| $V_1$ | S-060 | 41 | 0.150 |
| $V_1$ | S-072 | 39 | 0.082 |
| $V_1$ | S-073 | 35 | 0.020 |
| $VI_2$ | S-029 | 63 | 0.494 |
| $VI_2$ | S-030 | 63 | 0.544 |
| $VI_4$ | S-036 | 57 | 0.980 |
| $VI_3$ | S-041 | 62 | 0.619 |
| $VI_4$ | S-042 | 72 | 0.064 |

instantaneous shut-in pressure are not necessarily accurate. If the hydraulic fracturing method was still used to calculate the ground stress, a large deviation tended to be produced between the calculated result and practical case. The ground stress can also be obtained by using acoustic logging data [32, 33]:

$$\begin{cases} \sigma_H = \left(\dfrac{\mu}{1-\mu} + A\right)(\sigma_v - \varphi p_0) + \varphi p_0, \\ \sigma_h = \left(\dfrac{\mu}{1-\mu} + B\right)(\sigma_v - \varphi p_0) + \varphi p_0, \end{cases} \tag{3}$$

where $\mu$ is Poisson's ratio of the coal, $A$ and $B$ are the tectonic stress coefficients, $\sigma_v$ is a vertical stress (MPa), $\varphi$ is the pressure coefficient of the coal reservoir, and $p_0$ is the reservoir pressure (MPa).

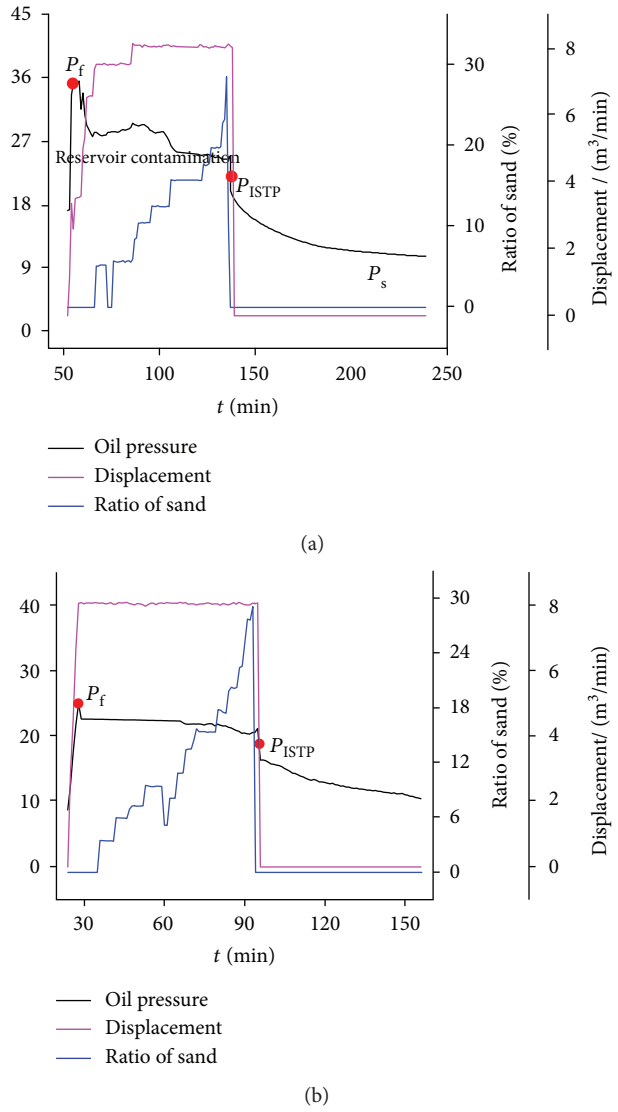


Figure 6: (a) The abnormal fracturing construction curves. (b) The normal fracturing construction curves.

Given that

$$\varphi = 1 - \frac{\rho\left(3V_p^2 - 4V_s^2\right)}{\rho_m\left(3V_{mp}^2 - 4V_{ms}^2\right)}, \tag{4}$$

where $\rho$ is the bulk density of coal (g/cm$^3$), $\rho_m$ is the skeletal density of coal (g/cm$^3$), $V_p$ and $V_s$ are vertical and transverse wave velocities (m/s), respectively, and $V_{mp}$ and $V_{ms}$ are the longitudinal and transverse velocities of the skeleton of the coal body (m/s).

When using log data for stress calculation, geological tectonic stress coefficients varied at different tectonic positions; to calculate the coefficients of the tectonic stresses in different positions, the same tectonic superimposed curve of normal fracturing wells was selected, and hydraulic fracturing was used to derive the in situ stress. Then, the vertical stress was calculated according to the density log and the depth of the

Table 2: The maximum and minimum principal stresses of partial CBM wells in different structural superposition zones.

| Zones | Well number | Fracturing pressure (MPa) | Tensile strength (MPa) | Reservoir pressure (MPa) | Maximum principal stresses stress (MPa) | Minimum principal stresses (MPa) | Tectonic stress coefficient *A* | Tectonic stress coefficient *B* |
|---|---|---|---|---|---|---|---|---|
| $I_2$ | S-010 | 22.09 | 0.25 | 3.95 | 27.70 | 17.83 | 1.55 | 0.87 |
| $I_2$ | S-011 | 25.78 | 0.28 | 3.85 | 32.09 | 20.48 | 1.53 | 0.88 |
| $I_3$ | S-058 | 19.57 | 0.24 | 1.53 | 27.14 | 16.00 | 1.61 | 0.89 |
| $I_1$ | S-117 | 21.64 | 0.20 | 7.73 | 23.30 | 17.54 | 1.56 | 0.87 |
| $I_4$ | S-124 | 21.77 | 0.24 | 5.23 | 26.10 | 17.62 | 1.58 | 0.86 |
| $II_4$ | S-005 | 18.33 | 0.50 | 3.85 | 31.99 | 20.38 | 1.36 | 0.71 |
| $II_3$ | S-018 | 10.07 | 0.52 | 3.90 | 7.88 | 7.11 | 1.35 | 0.70 |
| $II_4$ | S-019 | 14.57 | 0.51 | 3.22 | 13.47 | 10.25 | 1.37 | 0.69 |
| $II_2$ | S-064 | 14.47 | 0.51 | 2.52 | 14.42 | 10.30 | 1.39 | 0.68 |
| $II_1$ | S-085 | 24.82 | 0.49 | 7.62 | 28.47 | 20.14 | 1.38 | 0.68 |
| $III_3$ | S-015 | 24.78 | 0.28 | 2.44 | 36.33 | 21.09 | 1.52 | 0.74 |
| $III_3$ | S-020 | 22.99 | 0.28 | 2.48 | 37.30 | 20.83 | 1.53 | 0.79 |
| $III_2$ | S-044 | 20.99 | 0.26 | 1.80 | 27.87 | 16.80 | 1.55 | 0.76 |
| $III_2$ | S-062 | 18.48 | 0.25 | 2.10 | 19.06 | 13.13 | 1.52 | 0.77 |
| $III_1$ | S-090 | 27.46 | 0.28 | 2.38 | 40.82 | 23.46 | 1.56 | 0.78 |
| $IV_4$ | S-008 | 16.38 | 0.55 | 4.37 | 11.54 | 10.58 | 0.82 | 0.47 |
| $IV_4$ | S-013 | 18.84 | 0.51 | 4.30 | 20.93 | 14.52 | 0.80 | 0.45 |
| $IV_1$ | S-034 | 21.00 | 0.47 | 2.96 | 29.46 | 17.65 | 0.83 | 0.49 |
| $IV_1$ | S-035 | 23.86 | 0.44 | 3.35 | 32.09 | 19.62 | 0.85 | 0.48 |
| $IV_3$ | S-040 | 10.62 | 0.53 | 2.57 | 9.21 | 7.29 | 0.82 | 0.46 |
| $V_2$ | S-050 | 18.32 | 0.26 | 2.69 | 13.60 | 11.45 | 0.92 | 0.31 |
| $V_2$ | S-051 | 17.05 | 0.28 | 2.68 | 16.40 | 11.95 | 0.93 | 0.30 |
| $V_1$ | S-060 | 19.11 | 0.30 | 2.78 | 22.84 | 14.81 | 0.90 | 0.32 |
| $V_1$ | S-072 | 17.94 | 0.28 | 2.31 | 21.13 | 13.70 | 0.93 | 0.32 |
| $V_1$ | S-073 | 19.39 | 0.25 | 7.67 | 20.44 | 15.75 | 0.93 | 0.31 |
| $VI_2$ | S-029 | 24.45 | 0.47 | 2.77 | 27.28 | 18.01 | 1.26 | 0.70 |
| $VI_2$ | S-030 | 24.44 | 0.47 | 3.54 | 29.64 | 19.05 | 1.28 | 0.69 |
| $VI_4$ | S-036 | 21.28 | 0.42 | 4.79 | 29.85 | 18.50 | 1.29 | 0.68 |
| $VI_3$ | S-041 | 23.62 | 0.46 | 3.99 | 29.04 | 18.73 | 1.26 | 0.69 |
| $VI_4$ | S-042 | 13.89 | 0.53 | 2.83 | 16.45 | 10.88 | 1.27 | 0.70 |

coal seam. Poisson's ratio was found from longitudinal and transverse wave data. The tectonic stress coefficients *A* and *B* in different superimposed areas were obtained, based on which the maximum and minimum principal stresses on an abnormal CBM well were obtained using the acoustic logging method (Table 2).

Table 2 shows that the stress coefficients of the superimposed areas with different tectonic conditions varied. The tectonic stress coefficient of the superimposed areas of different synclines and anticlines is the largest. The tectonic stress coefficients for the superimposed areas of the wings of different synclines or different anticlines and the wings of different synclines and anticlines are moderate. The tectonic stress coefficients for the superimposed areas of the wings of different synclines or anticlines are minimal. Therefore, it is necessary to divide the tectonic superimposed area first when calculating the stress on a CBM well. Then, the maximum and minimum principal stresses were calculated according to the corresponding tectonic stress coefficients.

*4.3. The Relationship between Stress Difference and Permeability.* Here, the permeability of coal reservoir in the superimposed areas of different tectonic regions was calculated by using the method combining acoustic well logging, GSI, and *in situ* measurement. The maximum and minimum principal stresses were calculated by using hydraulic fracturing and acoustic logging techniques; the relationship between the stress difference and permeability is shown in Figure 7(a) when it is not divided into superimposed zones. The relationship between stress difference and permeability is shown in Figures 7(b)–7(g) when it is divided into superimposed zones.

Figure 7 indicates that the relationship between stress difference and permeability is not clear when tectonically superimposed areas were not divided. The permeability

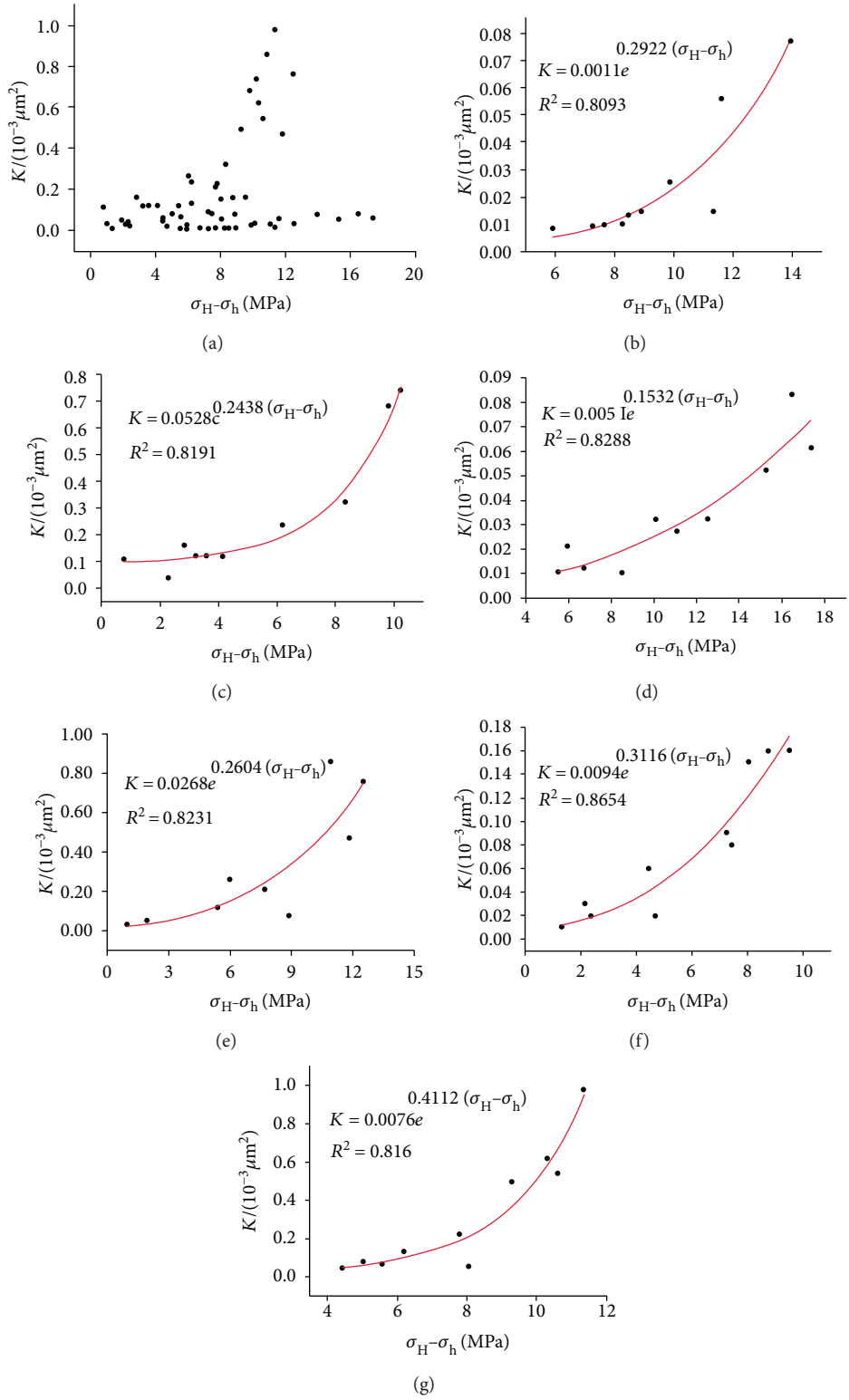


Figure 7: (a) The relationship between the stress difference and permeability not divided into superimposed zones. (b) The relationship between the stress difference and permeability on the Zone I. (c) The relationship between the stress difference and permeability on the Zone II. (d) The relationship between the stress difference and permeability on the Zone III. (e) The relationship between the stress difference and permeability on the Zone IV. (f) The relationship between the stress difference and permeability on the Zone V. (g) The relationship between the stress difference and permeability on the Zone VI.

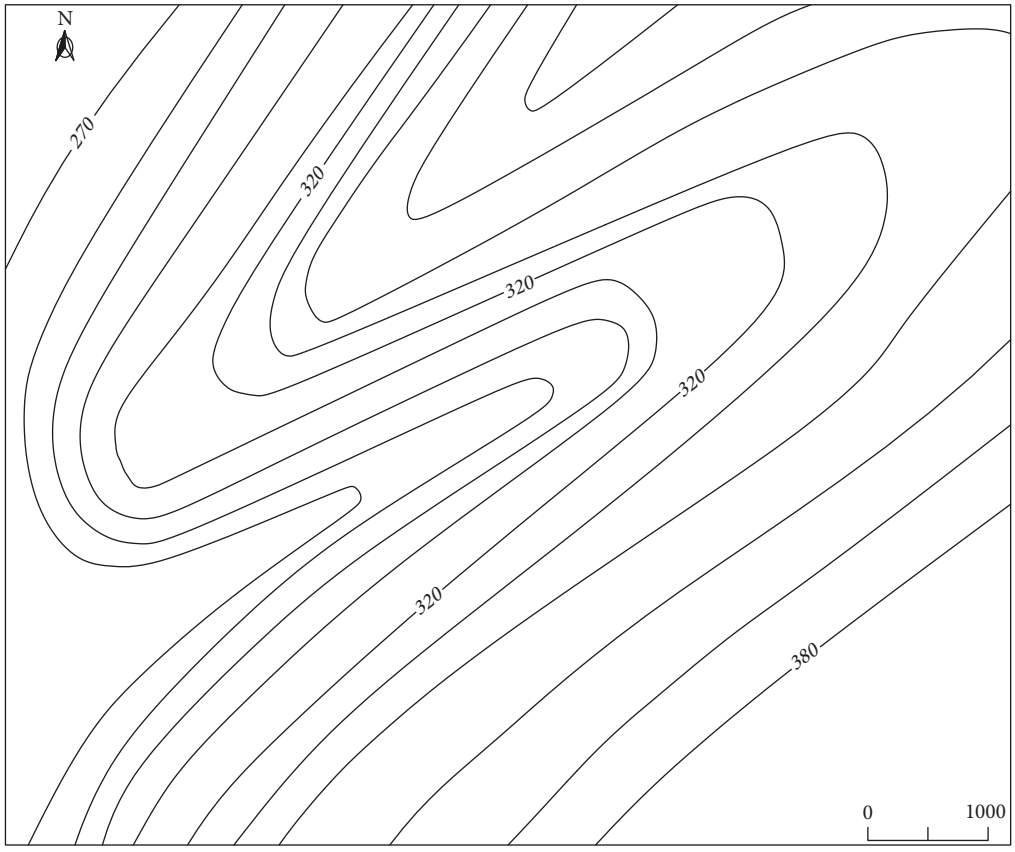


Figure 8: The structural features of the coal seam at key moments in the Yanshanian period.

increases exponentially with increasing stress difference when tectonically superimposed areas were divided. The tectonic superpositions are different with differing growth trends.

*4.4. Controlling Effect on Permeability and Stress of Coal Seam under Different Tectonic Movement Conditions.* In this area, the no. 3 coal seam underwent multistage tectonic movement; results show that the research area was mainly affected by the near-horizontal compressive stress imposed in the Yanshanian period. The direction of the stress was mainly NW-SE, and the structural features of the coal seam at key moments can be obtained by levelling survey (Figure 8).

As seen in Figure 8, the anticline and syncline folds in NNE direction were formed due to the Yanshanian tectonic movement. The deformation of the coal seam was large as seen in cores from different anticlines or synclines. The coal structure was mainly cataclastic with a high permeability. The coal seam was located below the neutral surface of the fold; the core of the syncline was subjected to tensile stress which was low and partially released from the core, and the stress therein was relatively low. The core of the anticline was under relatively concentrated extrusion stress. The deformation of the coal seam was lower in the wings of different synclines or anticlines. The coal structure was mainly composed of primary coal with relatively low permeability, and it was subjected to moderate stress.

The southern section of Shizhuang was mainly affected by the near-horizontal compressive stress striking NNE-SSW in the early Himalayan period. The superposition continues to cause deformation. The tectonics of the research region in the period after the early Himalayan are shown in Figure 9.

The alternate anticline and syncline in NEE direction were formed in the early Himalayan period. The structural features of the coal seam in different superimposed areas such as the cores of different anticlines, the superimposed areas of the wings of syncline or anticline, the cores of different synclines, the wings and the cores of different anticlines, and the wings and the cores of different synclines can be formed by superposition on the original structures of the coal seam. The coal seam was further deformed in areas superimposed by the cores of the folds, and the coal structure was mainly granulated coal or mylonitised coal with the lowest permeability. The stress was further concentrated on superimposed areas formed by the cores of the different anticlines; the stress in these areas was the largest found. The deformation of the coal seam in superimposed areas of the wings and the cores of the folds affected the permeability. The difference of amplitude of anticlines and synclines led to differences in coal deformation in the superimposed areas in both the wings of the fold in north and central direction and southeast direction, and the permeability was thus different. The permeability in superimposed areas of the wings of different synclines or anticlines striking north-central direction resulted

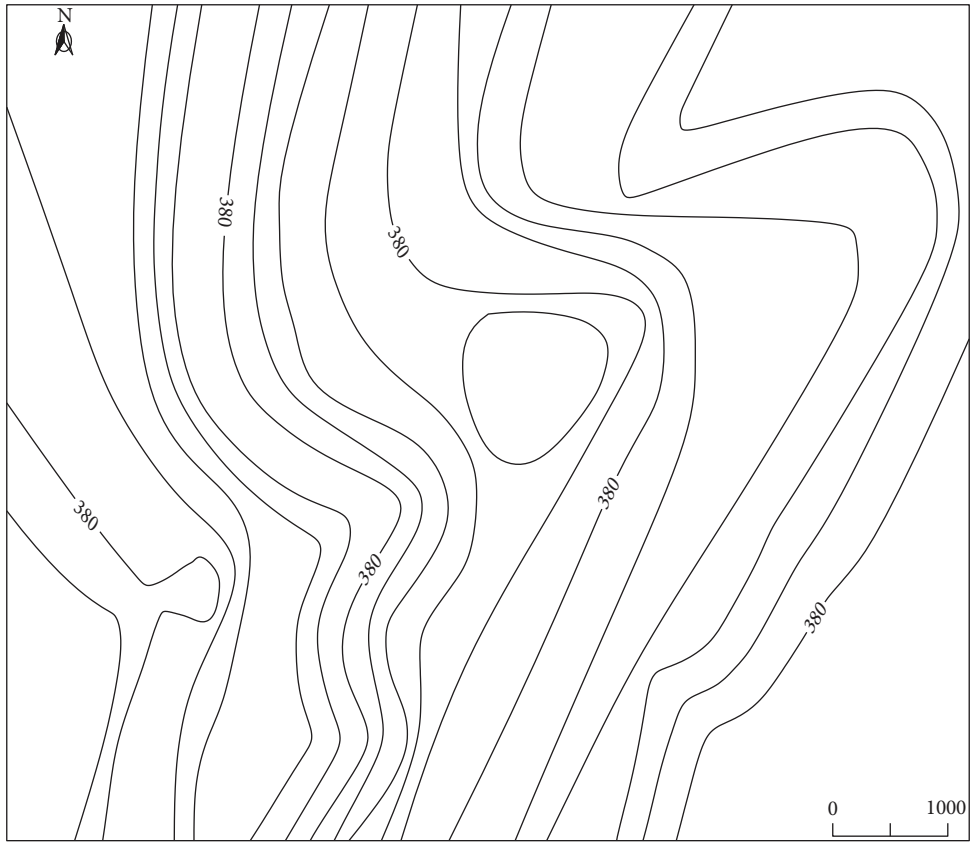


Figure 9: The structural features of the coal seam at key moments in the early Himalayan period.

in the maximum permeability, and the permeability in the superimposed areas of the wings of different synclines or anticlines in a southeasterly direction was lower than that in the superimposed areas of the wings and the cores of the fold.

The area was mainly affected by the near-horizontal compressive stress in the late Himalayan period. The direction of the stress was mainly NEE-SWW; the tectonic features of the coal seam were obvious in the southeast, and the other areas were less clear. This area was also affected by the tectonic stress in the S-N direction; the tectonic features in the northeastern area were obvious. Therefore, the tectonic movement in the Yanshanian period and the early Himalayan period generally led to the current stress-permeability regime which was generally exponential.

## 5. Conclusions

(1) The permeability of the coal seam can be quantitatively evaluated using a combined method integrating the geological strength index (GSI), acoustic logging curves, and in situ measurement. The method was confirmed by calculating hydraulic fracturing stress and acoustic logging curve method which can avoid errors resulting from the selection of engineering parameters or difficulty in choosing a stress coefficient in different tectonic sites; the calculated results were closer to the real values

(2) Multistage tectonic movements led to complex changes in coal permeability and stress with strong heterogeneity in block-scale permeability. The relationships between different stresses and permeability were not obvious without dividing tectonically superimposed areas. When the tectonically superimposed areas were divided, the permeability increased exponentially with the increase of stress in different tectonically superimposed areas

(3) The deformation of the coal seams were different in different superimposed areas, while the differences in their permeability were large; the deformation of the coal seam in superimposed areas, in the cores of different anticlines or synclines, was the greatest, and the coal structure was mainly granulated coal or mylonitised coal with the lowest permeability. The deformation of coal seams in the superimposed areas of the wings of different fold belts was different due to differences in the amplitudes of anticlines and synclines, and the changes in permeability were large. The deformation of coal seams in the superimposed areas on the wings of fold belts striking north-central direction was relatively weak, and its permeability was the highest. The permeability in the superimposed areas of the wings of different fold belts in a southeasterly direction was lower than that in the superimposed areas of the wings and the cores of folds

(4) The differences between the amplitudes and wavelengths of the same folded zones, including the superimposed areas formed by the different wings of the folds and the cores of different synclines, led to different deformations of the coal seams and changes in the stresses therein. The relationships between the deformation, stress, and permeability warranted further research in the future. These results can offer guidance to those interested in the engineering of CBM wells

## Data Availability

The data used to support the findings of this study are available from the corresponding author upon request.

## Conflicts of Interest

The authors declare no competing financial interest.

## Acknowledgments

This study was supported by the Major National Oil and Gas Projects (2017ZX05064-003-001), the Program for Innovative Research Team in University of Ministry of Education of China (IRT_16R22), the China Innovative Talents of Henan Province Science and Technology project (15HASTIT050), and the Central Plains Economic Zone of coal seam gas (Ye Yan) Henan Collaborative Innovation Center support.

## References

[1] G. Wang, Y. Qin, J. Shen, L. J. Zhao, J. C. Zhao, and Y. P. Li, "Accumulation effects and coupling relationship of deep coalbed methane," *Acta Petrolei Sinica*, vol. 35, pp. 462–468, 2014.

[2] S. H. Zhang, S. H. Tang, Y. Wan, and G. Q. Shu, "Changes in adsorption swelling properties and dynamic permeability of coals under triaxial confining pressure," *Geological Journal of China Universities*, vol. 18, pp. 539–543, 2012.

[3] Y. J. Meng, D. Z. Tang, H. Xu, W. M. Shen, and J. L. Zhao, "Progress and prospect of gas-water relative permeability of coal and rock," *Coal Science and Technology*, vol. 42, pp. 51–55, 2014.

[4] G. Worotnicki and R. Walton, "Triaxial "hollow inclusion" gauges for determination of rock stresses in situ," in *Symposium on Investigation of Stress in Rock: Advances in Stress Measurement*, pp. 1–8, Sydney, NSW, 1976.

[5] P. F. Shan, F. Cui, J. T. Cao, X. P. Lai, H. Sun, and Y. R. Yang, "Testing on fluid-solid coupling characteristics of fractured coal-rock mass considering regional geostress characteristics," *Journal of China Coal Society*, vol. 43, pp. 105–117, 2018.

[6] X. M. Ni, Z. H. Li, Y. B. Wang, and J. G. Wu, "Favorable sections optimization about coalbed methane on developing fault blocks in central of Qinshui Basin," *Natural Gas Geoscience*, vol. 28, pp. 602–610, 2017.

[7] J. R. E. Enever and A. Henning, "The relationship between permeability and effective stress for Australian coals and its implications with respect to coalbed methane exploration and reservoir modelling," in *1997 International Coalbed Methane Symposium*, pp. 13–22, Tuscaloosa, AL, USA, May 1997.

[8] Z. Q. Li, X. F. Xian, L. J. Xu, and D. X. Jia, "Quantitative predicting method of coalbed methane relative high permeability regioningeo-stress and geothermal field," *Journal of China Coal society*, vol. 34, pp. 766–770, 2009.

[9] H. Zhang, Y. Z. Wang SZ Zhen, X. L. Jin, and G. H. Li, "Palaeotectonic stress-fields and prediction of higher-permeability region for coalbed methane exploration in low-permeability coal reservoirs," *Journal of China Coal society*, vol. 36, pp. 708–711, 2004.

[10] D. M. Liu, S. D. Zhou, Y. D. Cai, and Y. B. Yao, "Study on effect of geo-stress on coal permeability and its controlling mechanism," *Coal Science and Technology*, vol. 45, pp. 1–8+23, 2017.

[11] X. M. Ni, Y. C. Zhao, Y. X. Cao, and L. Gao, "Distribution characteristics of coal reservoir permeability under the action of tectonic movement in western Fukang mining area," *Coal Geology & Exploration*, vol. 45, pp. 40–45, 2017.

[12] Q. R. Meng, E. Wand, and J. M. Hu, "Mesozoic sedimentary evolution of the northwest Sichuan basin: implication for continued clockwise rotation of the South China block," *Geological Society of America Bulletin*, vol. 117, no. 3, pp. 396–410, 2015.

[13] P. Ian, "Coalbed methane completions: a world view," *International Journal of Coal Geology*, vol. 82, no. 3-4, pp. 184–195, 2010.

[14] S. D. Mohaghegh, "Reservoir modeling of shale formations," *Journal of Natural Gas Science and Engineering*, vol. 12, pp. 22–33, 2013.

[15] Z. P. Meng, *Development Geology Theory and Method of Coalbed Methane*, Science press, Beijing, 2010.

[16] S. C. Jones, "A technique for faster pulse-decay permeability measurements in tight rocks," *SPE Formation Evaluation*, vol. 12, no. 1, pp. 19–26, 1997.

[17] H. H. Liu, S. X. Sang, J. H. Xue et al., "Characteristics of an in situ stress field and its control on coal fractures and coal permeability in the Gucheng block, southern Qinshui Basin, China," *Journal of Natural Gas Science and Engineering*, vol. 36, pp. 1130–1139, 2016.

[18] X. M. Ni, Y. H. Yang, Y. B. Wang, and J. P. Ye, "Study on gas production and water production characteristics of CBM vertical wells under multi period tectonic movement of un-development fault in central south Qinshui Basin," *Journal of China Coal Society*, vol. 41, pp. 921–930, 2016.

[19] Q. Liu, *Research on Geophysical Logging Evaluation Method for Shale Gas Reservoir, [M.S. Thesis]*, University of Geosciences, Beijing, China, 2013.

[20] G. C. Zhang, J. G. Ren, Z. M. Song, B. Li, and G. F. Liu, "Vector calculation model and diffusion experiments of $CH_4$ for directional raw coal," *Journal of Henan Polytechnic University (Natural Science)*, vol. 34, pp. 593–599, 2015.

[21] S. Li, J. S. Chen, X. Y. Feng, B. Yang, and X. Y. Ma, "Catalytic pyrolysis of Huang Tu Miao coal: TG-FTIR study," *Journal of Fuel Chemistry and Technology*, vol. 41, pp. 271–276, 2013.

[22] V. Vishal, P. G. Ranjith, S. P. Pradhan, and T. N. Singh, "Permeability of subcritical carbon dioxide in naturally fractured Indian bituminous coal at a range of down-hole stress conditions," *Engineering Geology*, vol. 167, pp. 148–156, 2013.

[23] S. Liu and S. Harpalani, "Permeability prediction of coalbed methane reservoirs during primary depletion," *International Journal of Coal Geology*, vol. 113, pp. 1–10, 2013.

[24] S. H. Zhang, S. H. Tang, Z. C. Li, L. H. Qiao, and C. Men, "The hydrochemical characteristics and ion changes of the coproduced water: taking Shizhuangnan block, south of the Qinshui basin as an example," *Journal of China University of Mining & Technology*, vol. 44, pp. 292–299, 2015.

[25] X. B. Su and X. Y. Lin, *Coalbed Methane Geology*, Coal Industry Press, Beijing, 2009.

[26] E. Hoek and E. T. Brown, "Practical estimates of rock mass strength," *International Journal of Rock Mechanics and Mining Sciences*, vol. 34, no. 8, pp. 1165–1186, 1997.

[27] H. Y. Gou, X. B. Su, D. P. Xia, X. M. Ni, and G. S. Li, "Relationship of the permeability and geological strength index (GSI) of coal reservoir and its significance," *Journal of China Coal society*, vol. 35, pp. 1319–1322, 2010.

[28] M. Weber, T. H. Wilson, B. Akwari, A. W. Wells, and G. Koperna, "Impact of geological complexity of the Fruitland Formation on combined $CO_2$ enhanced recovery/sequestration at San Juan Basin pilot site," *International Journal of Coal Geology*, vol. 104, pp. 46–58, 2012.

[29] M. Zhao, H. Zhou, and D. Chen, "Investigation and application on gas-drive development in ultra-low permeability reservoirs," *Journal of Hydrodynamics*, vol. 20, no. 2, pp. 254–260, 2008.

[30] S. H. Tang, B. C. Zhu, and Z. F. Yan, "Effect of crustal stress on hydraulic fracturing in coalbed methane wells," *Journal of China Coal society*, vol. 36, pp. 65–69, 2011.

[31] B. C. Haimson and F. H. Cornet, "ISRM suggested methods for rock stress estimation-part 3: hydraulic fracturing (HF) and/or hydraulic testing of pre-existing fractures (HTPF)," *International Journal of Rock Mechanics and Mining Sciences*, vol. 40, no. 7-8, pp. 1011–1020, 2003.

[32] J. Li, M. Zha, and Z. Liu, "Research on crustal stress distribution based on acoustic logging data——taking North Region of Renqiu Ordovician Buried Hill of Raoyang Depression for example," *Rock and Soil Mechanics*, vol. 32, pp. 2765–2770, 2011.

[33] L. Scesi and P. Gattinoni, "Roughness control on hydraulic conductivity in fractured rocks," *Hydrogeology Journal*, vol. 15, no. 2, pp. 201–211, 2007.